Arch. Metall. Mater. **64** (2019), 3, 1195-1200

DOI: 10.24425/amm.2019.129513

K. TAVAEI*, A. MEYSAMI*#

EFFECTS OF V-Ti ON DYNAMIC RECRYSTALLIZATION BEHAVIOR AND HOT DEFORMATION ACTIVATION ENERGY OF 30MSV6 MICRO-ALLOYED STEEL

In the current study, the hot deformation of medium carbon V-Ti micro-alloyed steel was surveyed in the temperature range of 950 to 1150°C and strain rate range of 0.001 to 1 s^{-1} after preheating up to 1200°C with a compression test. In all cases of hot deformation, dynamic recrystallization took place. The influence of strain rate and deformation temperature on flow stress was analyzed. An increase in the strain rate and decrease in the deformation temperature postponed the dynamic recrystallization and increased the flow stress. The material constants of micro-alloyed steel were calculated based on the constitutive equations and Zener-Hollomon parameters. The activation energy of hot deformation was determined to be 458.75 kJ/mol, which is higher than austenite lattice self-diffusion activation energy. To study the influence of precipitation on dynamic recrystallization, the stress relaxation test was carried out in a temperature range of 950 to 1150°C after preheating up to 1200°C. The results showed no a stress drop while representing the interaction of particles with dynamic recrystallization.

Keywords: dynamic recrystallization; activation energy; hot compression; 30MSV6 micro-alloyed steel; flow stress

1. Introduction

Some micro-alloys are used widely in different industries such as automobiles and petroleum [1-3]. The main reason for using these steels is that there is no need for heat treatment after deformation, which creates advantages such as saving energy, time, and cost [4]. Compared with heat-treated low carbon steels, the micro-alloyed steels containing titanium and vanadium possess less toughness. The V-Ti micro-alloyed steel used in this study, i.e., 30MSV6, is considered as a promising alternative for quenched-tempered, controlled-rolling, and normalized steels in automotive industries and some other applications.

To improve the mechanical properties of micro-alloyed steels, hot deformation parameters should be exactly controlled. Dynamic recrystallization is the main mechanism of controlling microstructure during the hot deformation. Moreover, it plays a significant role in decreasing the stress level and is a powerful facility to control mechanical behavior in industrial processing. For this purpose, physical simulation is a suitable method for evaluation of dynamic recrystallization during hot deformation in laboratory scale. The physical simulation includes the exact reproduction of the thermo-mechanical processes in the laboratory that metal is exposed to in the actual fabrication or end use. In the physical simulation, hot compression and/or torsion tests are normally used to achieve the metal flow behavior and these data are further used to model the hot rolling of rod, bar, strip, plate and etc. The complete model developed for this purpose is expressed as a function of various variables such as temperature, strain, strain rate, inter-pass time, restoration process, pre-test thermal history, and potential for precipitation.

Wei et al. evaluated the behavior of dynamic recrystallization of vanadium micro-alloyed at various temperatures. Vanadium plays an important role in the hot deformation of steel [5]. Gomez and Medina investigated the influence of important factors such as Ti/N ratio and Nb-Al content on the microstructure of hot rolled steels and showed that Niobium is an effective element on static recrystallization [6]. Badjena and Park illustrated that Al-V-N micro-alloyed steel accelerated dynamic recrystallization [7]. She et al. investigated hot deformed Mn-Nb micro-alloyed steel in order to determine the controlled rolling of steel parameters [8].

Accordingly, it is important to realize the hot deformation of micro-alloyed steels. Also, precipitation of carbonitrides during hot deformation occurs and controls the dynamic recrystallization at high temperature.

Other ways of analyzing the effect of particles on dynamic recrystallization include stress relaxation. By the stress relaxation method, Wang et al. studied carbide precipitation behavior of Mo-Ti micro-alloyed steel [9]. Many researchers have worked on stress relaxation on micro-alloyed steel as well [10-13]. By calculating the activation energy of hot deformation and comparing it with austenite lattice self-diffusion activation energy [5,8], the effect of carbonitrides on dynamic recrystallization can be understood.

* GOLPAYEGAN UNIVERSITY OF TECHNOLOGY, DEPARTMENT OF METALLURGY & MATERIALS ENGINEERING, P.B.: 87717-65651, GOLPAYEGAN, IRAN

Corresponding author: meysami@gut.ac.ir

In the present study, the influence of two strong carbide former elements (i.e., Ti and V) on the dynamic recrystallization kinetics of a micro-alloyed steel is investigated. Due to the great influence of dynamics recrystallization on hot deformation flow stress and its effects on properties and microstructure of 30MSV6 micro-alloyed steel after processing, the prediction of characteristic points of the flow curves and determination hot deformation behavior is quite necessary for the modeling of the industrial hot working process. Hot deformation parameters are discussed using Zener-Hollomon's parameters and constitutive equations. The Zener-Hollomon parameter can be used to explain the high-temperature strain of materials such as steel. The forming temperature and strain rate were combined and expressed by the Zener-Holloman parameter, i.e., $Z = \dot{\varepsilon} \exp\left(\frac{Q}{RT}\right)$, where $\dot{\varepsilon}$ is the strain rate, R the gas constant, T the temperature, and Q the related activation energy [13]. In this paper, the dynamic recrystallization kinetics of V-Ti micro-alloyed steel is discussed based on flow stress-strain curves. Also, the effects of particles on recrystallization are investigated by using activation energy and stress relaxation.

2. Materials and Experiments

The used micro-alloyed steel was produced by Iran Alloy Steel Co.; the composition of the steel is given in Table 1. Cylindrical specimens with a diameter of 10 mm and a height of 15 mm were machined. The hot compression test device was a model of Zwick/Roel and had a capacity of 25 ton with a temperature accuracy of 5°C. It was equipped with a resistance furnace, which had SiC elements and a temperature range of 0-1400°C. To prevent any friction between the component cross-section and the jaw of the hot compression device, mica sheet was used. First, the samples were held in 1200°C for 5 min and the then hot compression test was performed at temperatures of 950, 1000, 1050, 1100, and 1150°C for 5 min; then samples were quenched in water immediately (Fig. 1). For stress relaxation test, the samples were preheated up to 1200°C for 5 min and tested with a strain of 0.15 and a strain rate of 0.1 s^{-1}. Afterward, the stress was analyzed with the passing of time at various temperatures and finally quenched in water. For the analysis of particles, the water-quenched samples were cut in the direction of pressure and then polished.

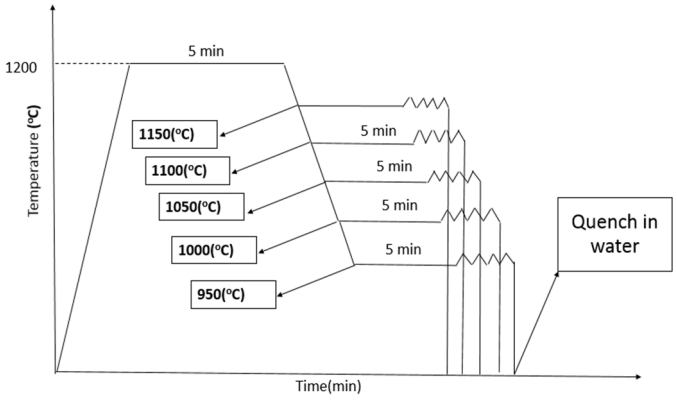

Fig. 1. Operation cycle of hot compression test

TABLE 1

Chemical composition of 30MSV6 micro-alloyed steel (w.t %)

Fe	C	Mn	Si	S	Ni
Base metal	0.329	1.430	0.530	0.057 (Max.: 0.060)	0.035
P	Cr	V	Ti	Cu	N
0.015 (Max.: 0.025)	0.223	0.095	0.025	0.034	0.012 (Max.: 0.015)

3. Results and Discussion

3.1. Stress-strain curves

Flow stress curves of 30MSV6 micro-alloyed steel at temperatures range of 950 to 1150°C and strain rates of 1 to 0.001 s^{-1} are shown in Fig. 2.

First, by applying the strain, the flow stress was increased up to peak stress and then decreased into different conditions in which strain variations are insignificant; i.e., steady-state conditions. As shown in Fig. 2 and Fig. 3, with an increment in the strain rate and decrement in the deformation temperature, the flow stress and peak stress have enhanced in the stress-strain curves due to the postponement of the dynamic recrystallization [8]. The decrease in the temperature of hot deformation decreased the recrystallization rate and increased the work hardening [8,14].

3.2. Physical simulation of flow stress by basic equations

The relationship between flow stress, absolute temperature (T) and strain rate ($\dot{\varepsilon}$) is presented by Arrhenius equation at high temperatures [15]. Therefore, the effects of temperature and strain rate on deformation behavior can be calculated by Zener-Holloman parameters (Z), as in the following equations [16-18]:

$$Z = \dot{\varepsilon}\left(\frac{Q}{RT}\right) \tag{1}$$

$$\dot{\varepsilon} = A_1 {\sigma_p}^{n1} \exp\left(\frac{Q}{RT}\right) \tag{2}$$

$$\dot{\varepsilon} = A_2 \exp\left(\beta\sigma_p\right)\exp\left(\frac{Q}{RT}\right) \tag{3}$$

$$\dot{\varepsilon} = A\left(\sinh\left(\alpha\sigma_p\right)\right)^n \exp\left(\frac{Q}{RT}\right) \tag{4}$$

where R, T, Q, σ_p and $\dot{\varepsilon}$ are gas constant, absolute temperature, activation energy of hot deformation, peak stress and strain rate, respectively. The values of these constant parameters are function of physical properties, crystal structure and composition of mate-

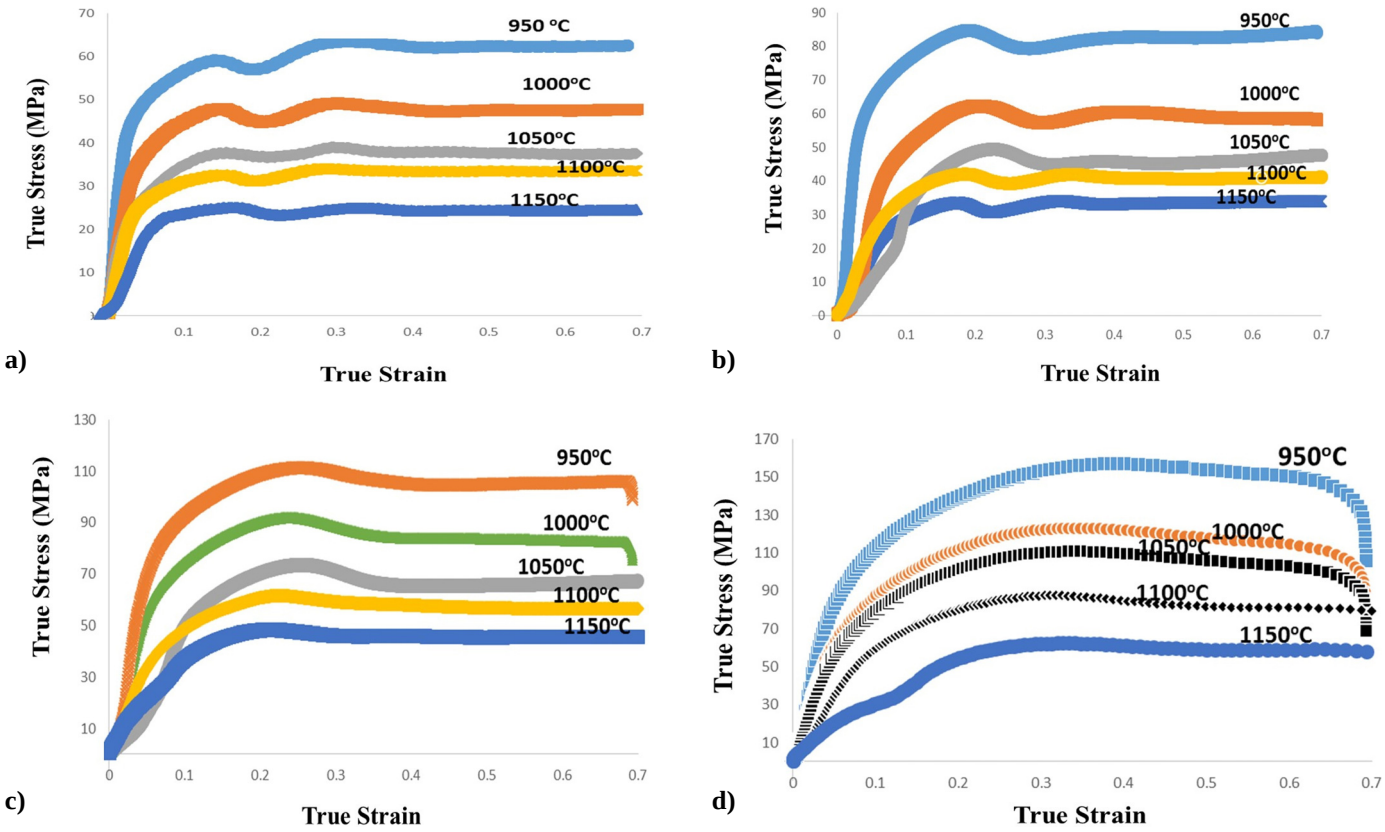

Fig. 2. Flow stress-strain curves at various temperatures and strain rates: (a) 0.001 s^{-1}, (b) 0.01 s^{-1}, (c) 0.1 s^{-1}, (d) 1 s^{-1}

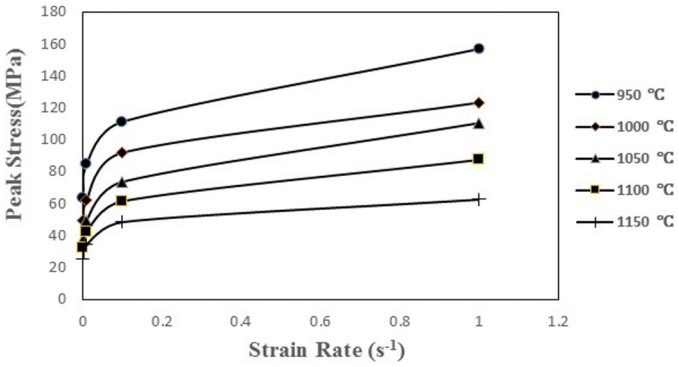

Fig. 3. Variations of peak stress versus strain rate at various temperatures

rial. The crystal structure has the most effect on these constant parameters, therefore in metals with allotropic structures they are temperature dependent. Steels have a FCC structure in the temperature range of 912 to 1394°C, therefore can assume they are constant in this temperature range.

By replacing Equations (2), (3) and (4) in Equation (1), Equations (5), (6) and (7) are obtained:

$$Z = A_1\sigma_p^{n1} = \dot{\varepsilon}\exp\left(\frac{Q}{RT}\right) \tag{5}$$

$$Z = A_2\exp\left(\beta\sigma_p\right) = \dot{\varepsilon}\exp\left(\frac{Q}{RT}\right) \tag{6}$$

$$Z = A\left(\sinh\left(\alpha\sigma_p\right)\right)^n = \dot{\varepsilon}\exp\left(\frac{Q}{RT}\right) \tag{7}$$

By taking natural logarithms of each side of Equations (5), (6) and (7), Equations (8), (9) and (10) are obtained:

$$Ln\dot{\varepsilon} + \left(\frac{Q}{R.T}\right) = LnA_1 + n_1 Ln\sigma_p \tag{8}$$

$$Ln\dot{\varepsilon} + \left(\frac{Q}{R.T}\right) = LnA_2 + \beta\sigma_p \tag{9}$$

$$Ln\dot{\varepsilon} + \left(\frac{Q}{R.T}\right) = LnA + nLn\left(\sinh\left(\alpha\sigma_p\right)\right) \tag{10}$$

Under constant temperature conditions during hot deformation process, by taking derivatives from Equations (8), (9), and (10), Equations (11), (12), and (13) are obtained:

$$n_1 = \left[\frac{\partial Ln\dot{\varepsilon}}{\partial Ln\sigma_p}\right] \tag{11}$$

$$\beta = \left[\frac{\partial Ln\dot{\varepsilon}}{\partial \sigma_p}\right] \tag{12}$$

$$n = \left[\frac{\partial Ln\dot{\varepsilon}}{\partial Ln\left(\sinh\left(\alpha\sigma_p\right)\right)}\right] \tag{13}$$

According to Equations (11)-(13), by obtaining the slope of $Ln\varepsilon^0$ versus $Ln\sigma_p$, σ_p, and $Ln\sinh(\alpha\sigma_p)$, we obtain $n1$, β, and n, respectively. Figs. 4 to 6 illustrate the linear regression of these

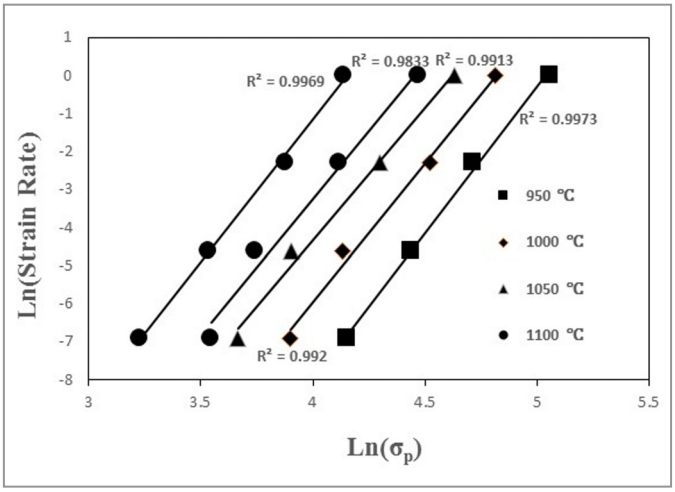

Fig. 4. Variations of $Ln\dot{\varepsilon}$ versus $Ln\sigma_p$ at various temperatures

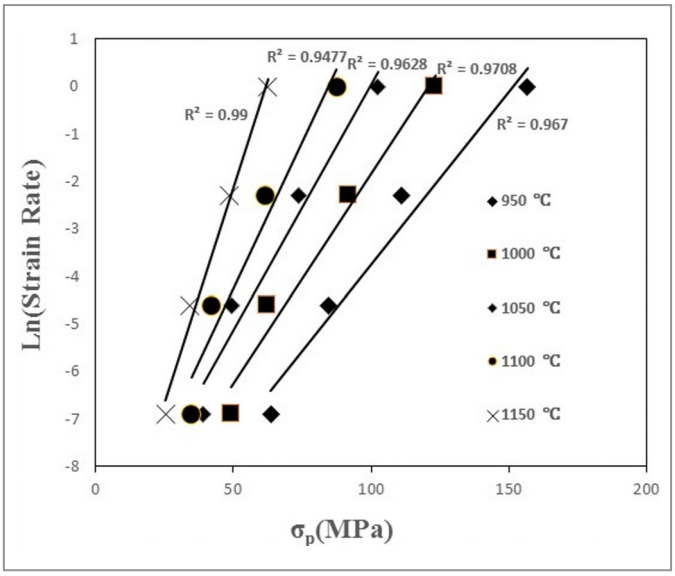

Fig. 5. Variations of $Ln\dot{\varepsilon}$ versus σ_p at various temperatures

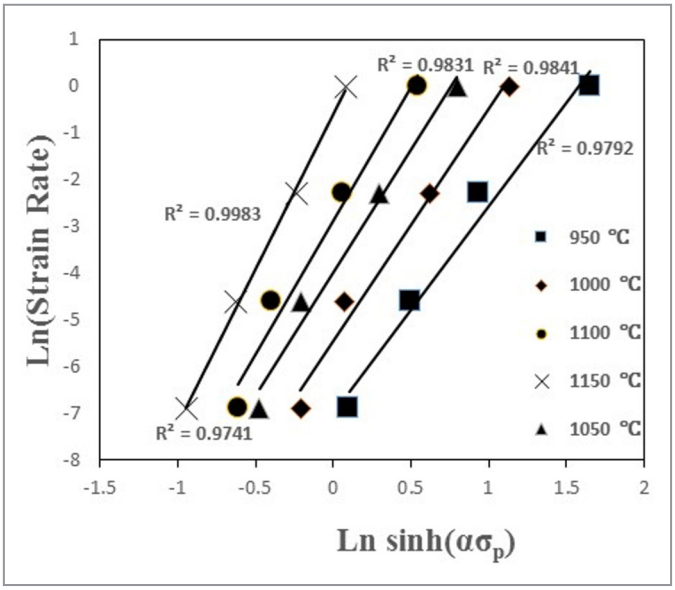

Fig. 6. Variations of $Ln\dot{\varepsilon}$ versus $Ln(\sinh(\alpha\sigma_p))$ at various temperatures

parameters at various temperatures. Also, α is achieved according to Equation (14):

$$\alpha = \frac{\beta}{n1} \tag{14}$$

Using linear regression plotted in Figs. 4 to 6, the material constants are calculated as n_1 =7.27, β = 0.11, n = 5.36, and α = 0.015.

3.3. Calculation of the activation energy of hot deformation

The activation energy of hot deformation at constant strain rates (Q) is derived from Equation (10):

$$Q = Rn\left[\frac{\partial Ln\left(\sinh\left(\alpha\sigma_p\right)\right)}{\partial\left(\frac{1}{T}\right)}\right] \tag{15}$$

Using slope of lines plotted in Fig. 7 and Equation (15), the average activation energy of hot deformation was calculated at various strain rates as 458.75 KJ/mol with a standard deviation equal to 72 KJ/mol. Wei et al. calculated this value equal to 273.225 KJ/mol for a medium carbon vanadium micro-alloyed steel [5]. In another investigation, this value was calculated as 420 KJ/mol for an Al-V -N micro-alloyed medium carbon steel [7]. Also, Shi et al. illustrated the activation energy for a Cr-Ni-Mo-Nb micro-alloyed steel is 386.06 KJ/mol [13].

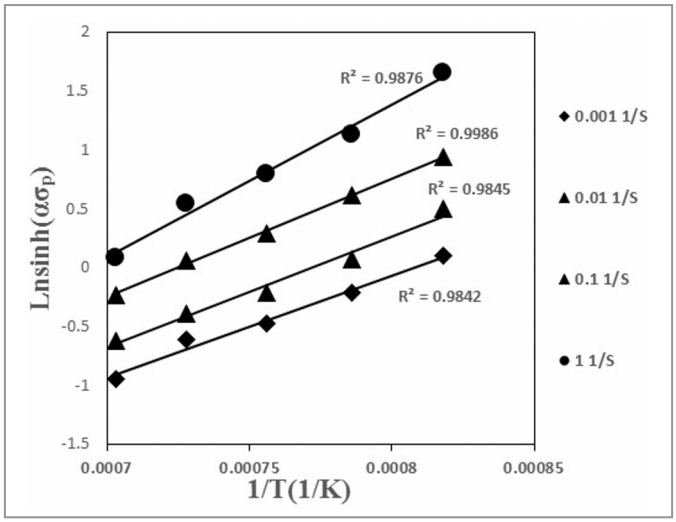

Fig. 7. Variations of $Ln(\sinh(\alpha\sigma_p))$ versus $1/T$ at various strain rate

The values of activation energy in 30MSV6 steel and in the mentioned investigations are higher than the austenite self-diffusion activation energy (270 KJ/mol). This indicates that the micro-alloyed elements increase the activation energy of hot deformation, also variation in the effective activation energy (as a function of the content of alloying elements) is completely similar to their influence on the self-diffusion activation energy [6].

The diagram of LnZ was plotted versus $Ln(\sinh(\alpha\sigma_p))$ to find the relationship between the Zener-Holloman parameter and peak stress (Fig. 8). In Fig. 8, stress has increased with enhancement of Zener-Holloman parameter. Therefore, the peak stress (σ_p) and the Zener-Holloman parameter (Z) have a direct relationship.

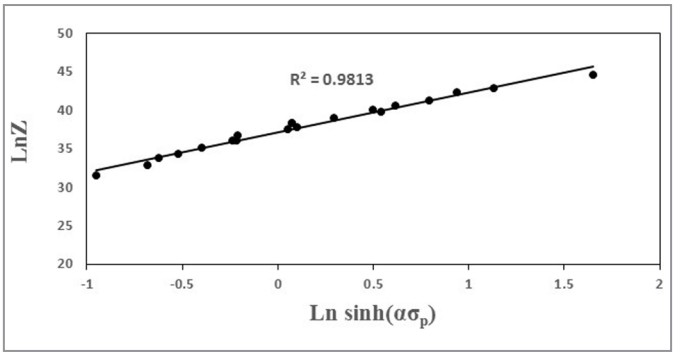

Fig. 8. Variations of LnZ versus $Ln(\sinh(\alpha\sigma_p))$

3.4. Evaluating of stress relaxation test

Fig. 9 shows the stress-time curves (stress relaxation) at 950, 1000, 1050, 1100, and 1150°C. It was found that there is a stress drop at the first stage but not a drop in the second stage. Also, according to Wang et al. [9] and Liu et al. [10], the lack of stress drop is related to the presence of micro-alloyed elements and interactions between dynamics recrystallization and precipitations. Increasing stress relief temperature from 950 to 1150°C decreased peak stress, which is related to the dynamic recrystallization kinetics due to temperature rising (Fig. 9) [8].

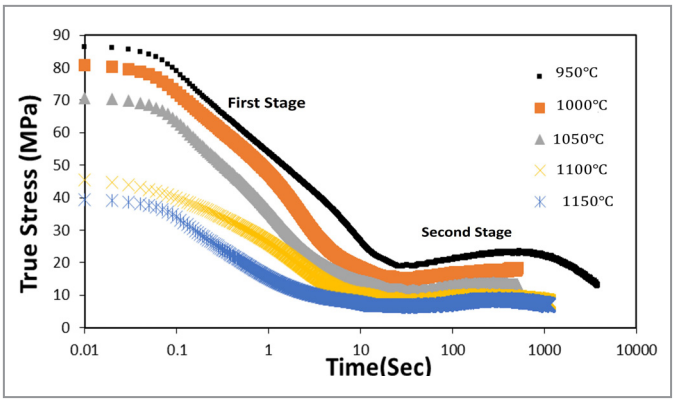

Fig. 9. Variations of true stress versus time at various temperatures

The identification image and EDS analysis of the intended precipitate by scanning electron microscopy (SEM) is shown in Fig. 10. The initial size of precipitate in micro-alloyed steel is about the size of a nanometre [19] while passing of time during stress relaxation causes the precipitate to become coarser [11]. As presented in Fig. 10, the precipitate size is about 3 μm. According to the Ostwald equation [20], surface tension causes small precipitates to dissolve and large one to grow; therefore, the particles of carbonitrides are coarse and due to increment of particles radius, the grain size of matrix increases [21-22]; therefore, it is not able to prevent the grain boundaries movement and then dynamic recrystallization will develop [23-24]. Also, as illustrated in Fig. 9, temperature rising increases growing of precipitation particles so that the interaction of particles with the recrystallization process will decrease.

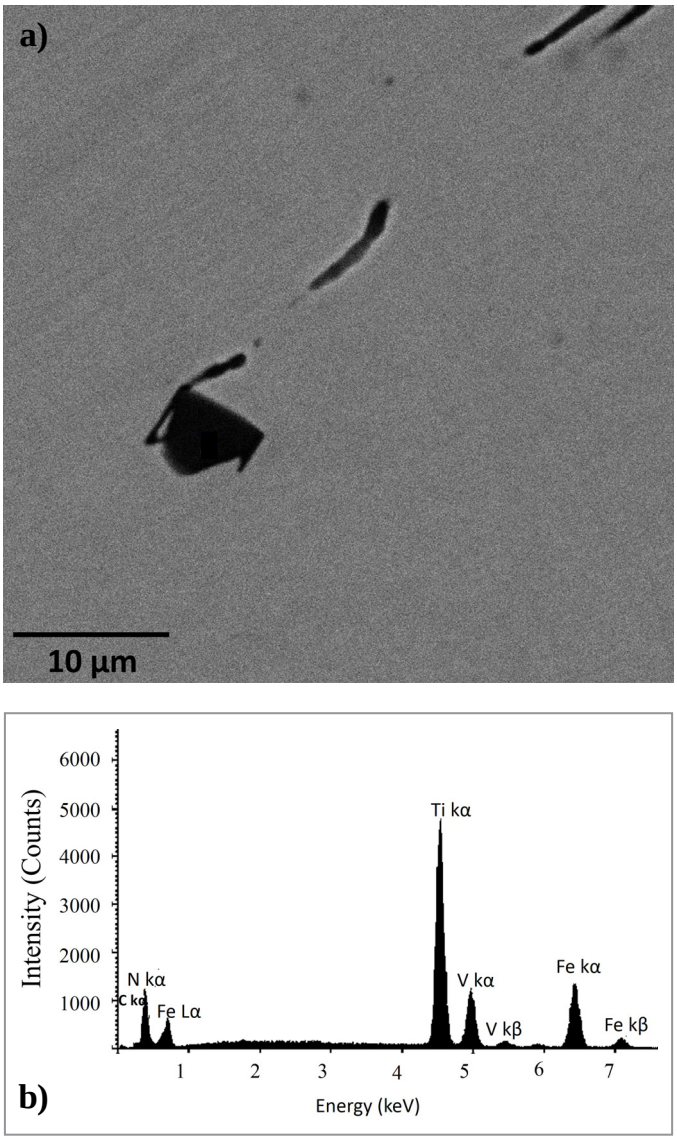

Fig. 10. (a): SEM image and (b): EDS analysis of the titanium precipitate

4. Conclusion

In the present study, a model was developed to predict dynamic recrystallization behavior of V-Ti micro-alloyed 30MSV6 steel during hot deformation using hot compression test in the temperature range of 950 to 1150°C at various strain rates. Based on the achieved results in this study, the conclusions of this study are as follows:

1. With an increase in the strain rate and decrease in deformation temperature, the intensity of stress peak in stress-strain curves was increased.

2. In all conditions of hot deformation, dynamic recrystallization occurred.
3. The Zener-Holloman parameter was obtained at various temperatures.
4. Average activation energy of steel was obtained to be $Q = 458.75 \pm 72$ KJ/mol.
5. Micro-alloying elements increase the activation energy of hot deformation.
6. The interaction between particles and recrystallization with stress relaxation test was observed.
7. An increase in the temperature decreases the amount of interaction of particles with the recrystallization process.
8. With the passage of time, the particles became coarser and dynamic recrystallization was developed.

Acknowledgment

The authors would like to thank the Iran Alloy Steel Company, Yazd-Iran, for providing the steels used in this research.

REFERENCES

[1] J.R. Davis, Alloying: Understanding the basics, 1st Edition, ASM International, Ohio (2001).

[2] S.H. Mohamadi Azghandi, V. Ghanooni Ahmadabadi, I. Raoofian, F. Fazeli, M. Zare, A. Zabett, H. Reihani, Mater. Design **88** (1), 751 (2015), DOI: 10.1016/j.matdes.2015.09.046.

[3] J. Wang, J. Chen, Z. Zhao, X. Ruan, J. Iron steel Res. Int. **15** (3), 78 (2008), DOI: 10.1016/S1006-706X(08)60130-2.

[4] M.I. Equbal, P. Talukdar, V. Kumar, R.K. Ohdar, Procedia Mat. Sci. **6**, 674 (2014), DOI: 10.1016/j.mspro.2014.07.083

[5] H.L. Wei, G.Q. Liu, X. Xiao, M. Zhang, Mater. Sci. Eng. A **573**, 215 (2013), DOI:10.1016/j.msea.2013.03.009.

[6] M. Gomez, S. F. Medina, Int. J. Mater. Res. **102** (10), 1197 (2011), DOI: 10.3139/146.110585.

[7] S.K. Badjena, J.K. Park, Mater. Sci. Eng. A. **548** (30), 126 (2012), DOI:10.1016/j.msea.2012.03.102.

[8] Y. She, Z.H. Zhang, J. Yang, J.T. Ju, Mater. Sci. Forum **724**, 287 (2012), DOI: 10.4028/www.scientific.net/MSF.724.287.

[9] Z. Wang, X. Sun, Z. Yang, Q. Yong, C. Zhang, Z. Li, Y. Weng, Mater. Sci. Eng. A **573**, 84 (2013), DOI: 10.1016/j.msea.2013.02.056.

[10] W.J. Liu, J.J. Jonas, Metal. Trans. A **19** (6), 1403 (1988).

[11] W.J. Liu, J.J. Jonas, Metal. Trans. A. **19** (6), 1415 (1988).

[12] F.J. Humphreys, M. Hatherly, Recrystallization and related annealing phenomena. 2nd Edition. Elsevier Science Ltd, Oxford (2002).

[13] Z. Shi-li, C. Hua-zhen, Y. Jian-song, H. Wen-hao, Z. Guo-qu, J. Iron Steel Res. Int. **22** (3), 264 (2015), DOI:10.1016/S1006-706X(15)60040-1.

[14] X. Dong, Z. Miaoyong, T. Zhengyou, S. Chao, J. Wuhan Uni. Tech. Mater. Sci. **28** (4), 819 (2013), DOI: 10.1016/j.msea.2012.04.063.

[15] G.E. Dieter, Mechanical Metallurgy. Third edition. McGraw-Hill: NY (1976).

[16] J. Chandra, R.P. Srivastav, Constitutive Models of Deformation, 1st edition, SIAM, Philadelphia (1987).

[17] S. Akbari Mousavi, M. Meisami, Investigation on Zener-Holloman parameter of a medium carbon Low alloy 1Cr-1Mn-1Si-1.5Ni Under Hot Deformation Test, Proc. Metals 2010, Roznov pod Radhostem (Eds), Czech Republic (2010).

[18] H. J. McQueen, N.D. Ryan, Mater. Sci. Eng. A **322** (1-2), 43 (2002), DOI: 10.1016/S0921-5093(01)01117-0.

[19] S.H. Mohamadi Azghandi, V. Ghanooni Ahmadabadi, A. Zabett, Philosophical Magazine **94** (24), 2758 (2014), DOI: 10.1080/14786435.2014.932460.

[20] L. Ratke, P.W. Voorhees, Growth and Coarsening: Ostwald Ripening in Material Processing, Springer, Berlin Heidelberg (2013).

[21] Materials Science and Technology, Chapter 8, F.B. Pickering, High Strength Low Alloy Steels, Wiley-VCH Verlag GmbH & Co. KgaA (2006).

[22] T. Nishizawa, I. Ohnuma, K. Ishida, Materials Transaction, JIM **38** (11), 950 (1997), DOI: 10.2320/matertrans1989.38.950.

[23] S.F. Medina, A. Quispe, M. Gomez, Metall. Mater Trans. A **45**, 1524 (2014), DOI: 10.1007/s11661-013-2068-1.

[24] J.A. Mohallem, J.B. Martins, C.A. Martins, M.L.P. Machado, Metall. Mater. 68 (4), 435 (2015), DOI: 10.1590/0370-44672014680140.